Supplementary Materials

Probing the mechanisms of morphological evolution and phase selection of intermetallic compounds for impurity-tolerant processing of recycled Al alloys

Shikang Feng*[a,b], Mika Shearwood[c], Andrew Lui[a], Dominic Banks[c], Tim Nicholls[c], Sion Richards[c], Matthew D. Wilson[c], Patrick S. Grant[a], and Enzo Liotti[a]

[a] *Department of Materials, University of Oxford, Oxford, OX1 3PH, UK*
[b] *School of Engineering and Informatics, University of Sussex, Brighton, BN1 9RH, UK*
[c] *Science and Technology Facilities Council, Rutherford Appleton Laboratory, Harwell Science and Innovation Campus, Didcot, OX11 0DE, UK*

S1 Supplementary alloy preparation

Fig. S1 shows a schematic of how samples for synchrotron X-ray radiography were sectioned from an as-cast 1.2Fe or 2.5Fe alloy ingot. First, the sprue riser on the top of the disk ingot was removed. Then, the edge was machined to remove any surface oxide, and the disk was cut using wire electro-discharge machining (wire EDM) as indicated by the yellow dashed lines. Foil samples for synchrotron X-ray radiography were then sectioned from the ingot using wire EDM.

S2 Supplementary data processing and analysis

As shown in Fig. 3 in the main paper, there is easily resolvable and profound contrast in the liquid, arising from solute segregation during IMC formation and growth. This

*Corresponding author.
Email addresses: shikang.feng@materials.ox.ac.uk; shikang.feng@sussex.ac.uk (S. Feng).

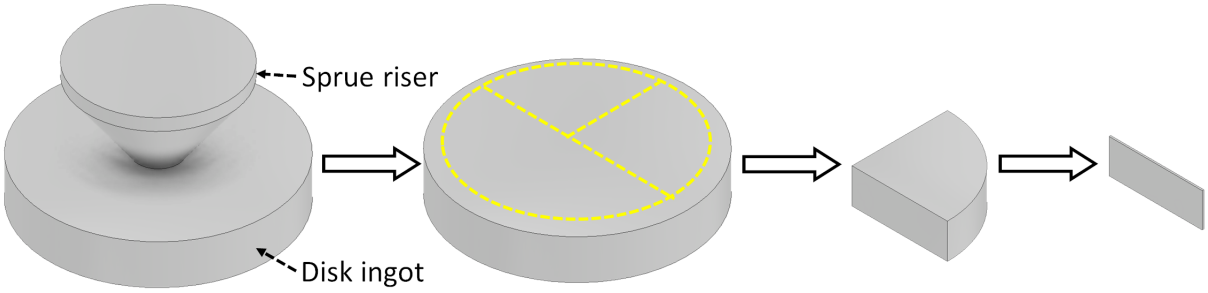

Figure S1: A schematic showing how samples for synchrotron X-ray radiography were sectioned from an as-cast 1.2Fe or 2.5Fe alloy ingot.

section describes the procedure followed to allow investigation of the Fe-depleted liquid fraction and its correlation with IMC phase selection in alloy 2.5Fe.

Although the 2.5Fe alloy is a multi-element alloy composed of Al, Si, Mg, Fe and Mn, X-ray absorption by Al, Si and Mg at the beam energy used (pink beam peaking at 25 keV) is negligible [1]. Further, the total Fe concentration in the liquid is > 6 times larger than Mn concentraiton (Table 1 in the main paper), and CALPHAD (CALculation of PHAse Diagram) simulation in Fig. S2 shows that both Fe and Mn segregate in the same trend during solidification. Therefore, it can be assumed that the X-ray absorption contrast in the liquid is dominated by the segregation (depletion in this case) of Fe. The X-ray radiographic images were processed in the following procedure to allow estimation of the Fe-depleted liquid fraction.

Flat fielding First, flat fielding was performed, where each image was divided by a flat image recorded when the sample was fully liquid and uniform. This step removed spatial variations in illumination and static artefacts (e.g. sample surface defects).

Global intensity scaling To study the evolution of the image intensity field during solidification, a global intensity scaling was performed [2, 3], following the flat fielding, on each image frame. For each experiment, each image frame was normalised between 0 and 1 using a set of global intensity minima and maxima. The global minima and maxima intensities were obtained by scanning through all the frames in the radiography sequence. A spatial bilateral filter [4] was then applied on each image for noise reduction

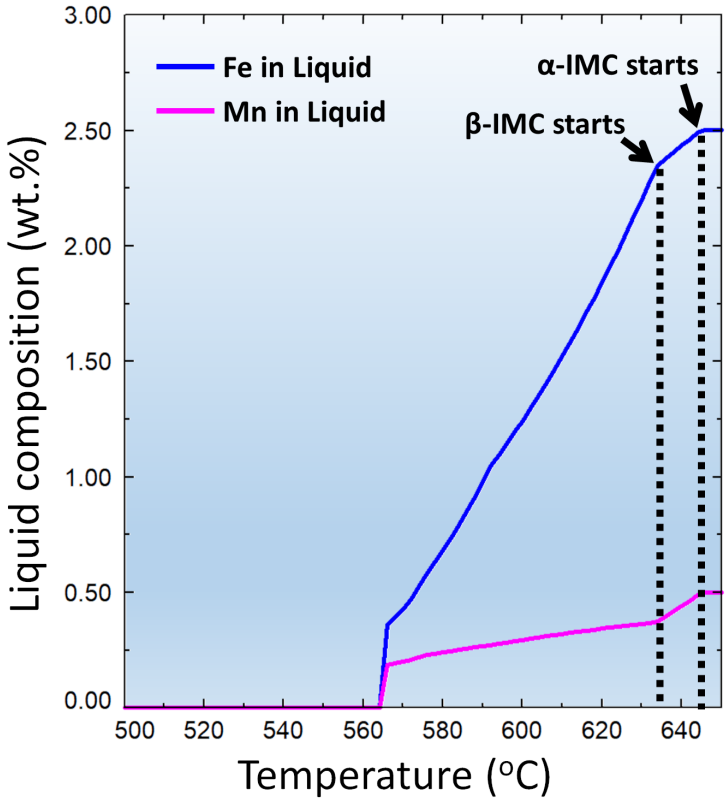

Figure S2: Fe and Mn concentrations in the liquid as a function of temperature for alloy 2.5Fe, calculated under equilibrium conditions using FactSage 8.2 and the FTlite database.

while preserving the edges of the IMC crystals (Fig. S3(a)).

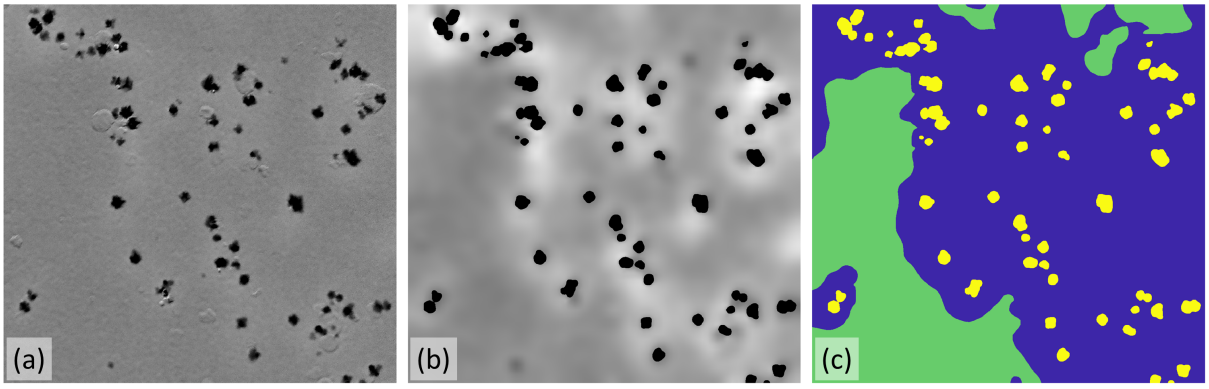

Figure S3: An example of image processing sequence for evaluation of the Fe depleted liquid fraction. (a) Image after flat fielding and global intensity scaling. (b) Image after segmentation to remove the solid IMC crystals. (c) False colour map after image subtraction by a flat reference image acquired when the sample was in a uniform liquid state. The blue area indicates the Fe-depleted liquid, defined as pixels in the liquid where the greyscale intensity change $\Delta I > \Delta I^* = 0.03$.

Image segmentation Images were smoothed by applying a diffusion filter [5, 6] and image segmentation was then performed to remove the solid IMC crystals in each frame

(Fig. S3(b)), following a well established procedure presented in details in [1–3, 7]. In Fig. S3(b), the area with a higher intensity (brighter) indicates liquid that was more depleted in Fe.

Fe depleted liquid fraction To facilitate the evaluation of the solute depletion effect arising from the interaction between an ensemble of IMCs, image subtraction was performed, where each image was subtracted by a flat reference image acquired before the start of each solidification sequence, with a uniform solute field. The resultant image in Fig. S3(c), with pixel value of ΔI, indicated the Fe depletion as the IMC crystals formed:

$$\Delta I = I_i - I_0 \tag{S1}$$

where I_i is the pixel intensity in the frame of interest, and I_0 is the pixel intensity of the flat reference image. The Fe-depleted liquid was defined as pixels in the liquid where $\Delta I > \Delta I^* = 0.03$, and is coloured blue in Fig. S3(c).

S3 Supplementary results

To further study the IMC phase selection in alloy 2.5Fe at higher cooling rates beyond those achievable in the synchrotron rig, a rod sample (8 mm diameter) of the alloy was cast in a water-cooled copper mould (cooling rate $\sim$100 K s^{-1}). Fig. S4 presents the as-cast microstructure, showing β-IMCs as the predominant IMC phase with very few α-IMCs.

Fig. S5 presents additional radiography sequences superimposed with instantaneous growth velocity fields, showing the growth of non-faceted, dendritic α-IMC phase in alloy 2.5Fe at 2 K s^{-1}.

Fig. S6 presents additional radiography sequences superimposed with instantaneous growth velocity fields, showing the growth of faceted, polyhedral α-IMC phase in alloy 2.5Fe at 0.5 K s^{-1}.

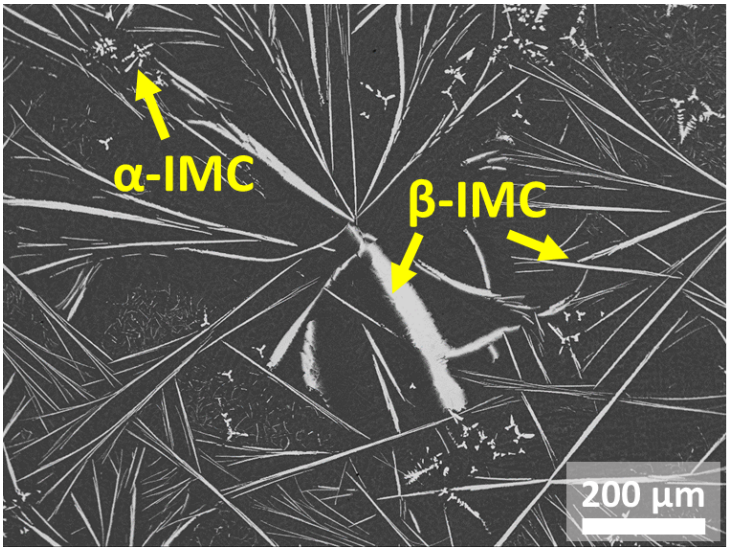

Figure S4: Microstructure of alloy 2.5Fe cast in a water-cooled copper mould.

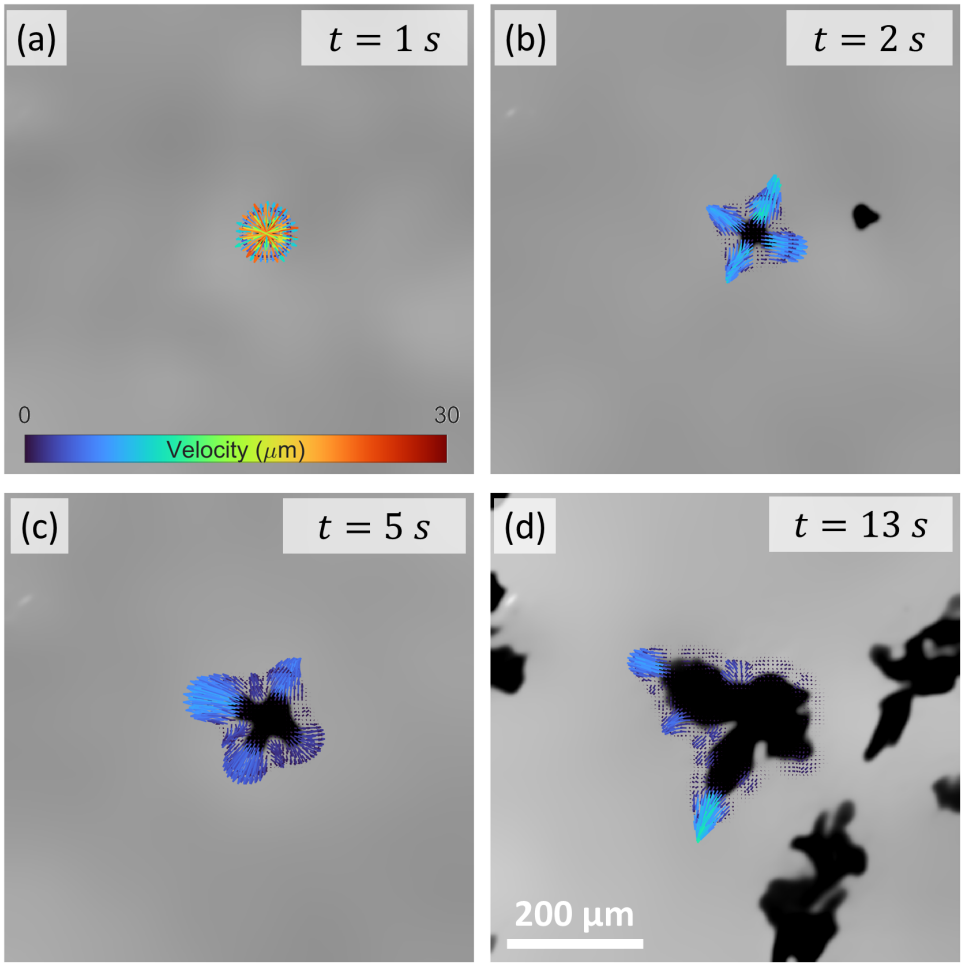

Figure S5: Additional radiography sequences superimposed with instantaneous growth velocity fields, showing the growth of non-faceted, dendritic α-IMC phase in alloy 2.5Fe at $2\,\mathrm{K\,s^{-1}}$.

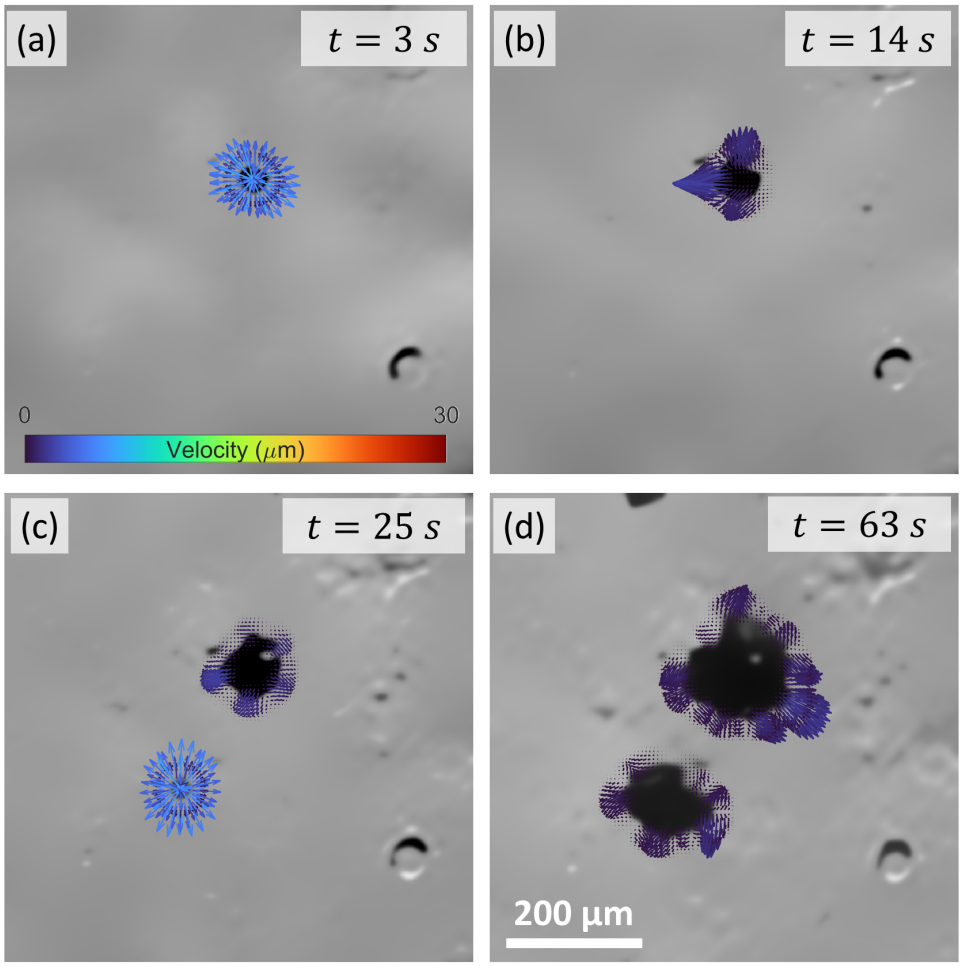

Figure S6: Additional radiography sequences superimposed with instantaneous growth velocity fields, showing the growth of faceted, polyhedral α-IMC phase in alloy 2.5Fe at $0.5\,\mathrm{K\,s^{-1}}$.

Post-solidification SEM images in Figs. S7(a) and (b) show exposed cross-sections of non-faceted, dendritic and faceted, polyhedral α-IMCs in alloy 2.5Fe, at $4\,\mathrm{K\,s^{-1}}$ and $0.5\,\mathrm{K\,s^{-1}}$, respectively.

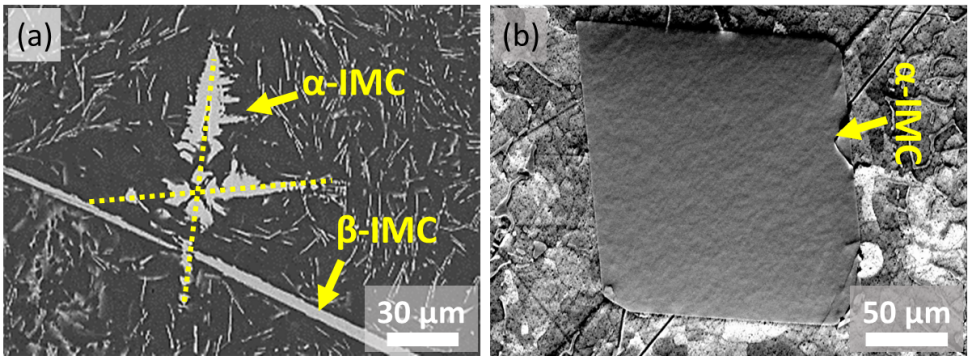

Figure S7: Post-solidification SEM images showing the exposed cross-sections of (a) non-faceted, dendritic and (b) faceted, polyhedral α-IMC phase in alloy 2.5Fe, solidified at $4\,\mathrm{K\,s^{-1}}$ and $0.5\,\mathrm{K\,s^{-1}}$, respectively. The yellow dashed lines in (a) indicate the primary arms of dendritic α-IMC.

References

[1] W. U. Mirihanage, K. V. Falch, I. Snigireva, A. Snigirev, Y. J. Li, L. Arnberg, R. H. Mathiesen, Retrieval of three-dimensional spatial information from fast in situ two-dimensional synchrotron radiography of solidification microstructure evolution, Acta Mater. 81 (2014) 241–247.

[2] E. Liotti, C. Arteta, A. Zisserman, A. Lui, V. Lempitsky, P. S. Grant, Crystal nucleation in metallic alloys using x-ray radiography and machine learning, Sci. Adv. 4 (4) (2018) eaar4004.

[3] S. Feng, E. Liotti, A. Lui, M. D. Wilson, P. S. Grant, Nucleation bursts of primary intermetallic crystals in a liquid Al alloy studied using in situ synchrotron X-ray radiography, Acta Mater. 221 (2021) 117389.

[4] C. Tomasi, R. Manduchi, Bilateral filtering for gray and color images, in: Proc. IEEE Int. Conf. Comput. Vis., IEEE, 1998, pp. 839–846.

[5] P. Perona, J. Malik, Scale-Space and Edge Detection Using Anisotropic Diffusion, IEEE Trans. Pattern Anal. Mach. Intell. 12 (7) (1990) 629–639.

[6] G. Gerig, O. Kbler, R. Kikinis, F. A. Jolesz, Nonlinear Anisotropic Filtering of MRI Data, IEEE Trans. Med. Imaging 11 (2) (1992) 221–232.

[7] E. Liotti, A. Lui, S. Kumar, Z. Guo, C. Bi, T. Connolley, P. S. Grant, The spatial and temporal distribution of dendrite fragmentation in solidifying Al-Cu alloys under different conditions, Acta Mater. 121 (2016) 384–395.